Bulk optical metamaterials assembled by microfluidic evaporation

Alexandre Baron,[1,2,*] Antonio Iazzolino,[3] Kévin Ehrhardt,[1,2] Jean-Baptiste Salmon,[3] Ashod Aradian,[1,2] Vasyl Kravets,[4] Alexander N. Grigorenko,[4] Jacques Leng,[3] Aurélie Le Beulze,[5] Mona Tréguer-Delapierre,[5] Miguel A. Correa-Duarte,[6] and Philippe Barois[1,2]

[1]CNRS, CRPP, UPR8641, F-33600, Pessac, France
[2]*Univ. Bordeaux, CRPP, UPR8641, F-33600, Pessac, France*
[3]*CNRS, University of Bordeaux, RHODIA, LOF, UMR5258, F-33600, Pessac, France*
[4]*University of Manchester, School of Physics and Astronomy, Manchester, United Kingdom*
[5]*CNRS, ICMCB, UPR9048, F-33600, Pessac, France*
[6]*Departamento de Quimica Fisica, Universidad de Vigo,36310, Vigo, Spain*
[*]*baron@crpp-bordeaux.cnrs.fr*

Abstract: We present high refractive index optical metamaterials assembled via a microfluidic evaporation technique. This technique enables fabrication of truly three-dimensional bulk samples from a suspension of nanoparticles with a number of layers well in excess of 600, surpassing rival techniques by at least an order of magnitude. In addition to their large dimensions, the assembled metamaterials show a high degree of homogeneity and warrant an easy and rapid optical characterization using spectroscopic ellipsometry. We believe that the suggested inexpensive method considerably reduces the complexity in assembling optical metamaterials and opens new avenues in engineering bulk optical devices by choice of nanoparticle composition and geometry.

OCIS codes: (160.0160) Materials; (160.3918) Metamaterials; (160.4236) Nanomaterials; (240.2130) Ellipsometry and polarimetry.

References and links

1. C. M. Soukoulis and M. Wegener, "Past achievements and future challenges in the development of three-dimensional photonic metamaterials," Nat. Photonics **5**, 523–530 (2011).
2. N. Liu, H. Guo, L. Fu, S. Kaiser, H. Schweizer, and H. Giessen, "Three-dimensional photonic metamaterials at optical frequencies," Nat. Mater. **7**(1), 31–37 (2008).
3. J. K. Gansel, M. Thiel, M. S. Rill, M. Decker, K. Bade, V. Saile, G. von Freymann, S. Linden, and M. Wegener, "Gold helix photonic metamaterial as broadband circular polarizer," Science **325**(5947), 1513–1515 (2009).
4. J. Valentine, S. Zhang, T. Zentgraf, E. Ulin-Avila, D. A. Genov, G. Bartal, and X. Zhang, "Three-dimensional optical metamaterial with a negative refractive index," Nature **455**(7211), 376–379 (2008).
5. T. Xu, A. Agrawal, M. Abashin, K. J. Chau, and H. J. Lezec, "All-angle negative refraction and active flat lensing of ultraviolet light," Nature **497**(7450), 470–474 (2013).
6. S. Mühlig, C. Rockstuhl, V. Yannopapas, T. Bürgi, N. Shalkevich, and F. Lederer, "Optical properties of a fabricated self-assembled bottom-up bulk metamaterial," Opt. Express **19**(10), 9607–9616 (2011).
7. L. Malassis, P. Massé, M. Tréguer-Delapierre, S. Mornet, P. Weisbecker, V. Kravets, A. Grigorenko, and P. Barois, "Bottom-up fabrication and optical characterization of dense films of meta-atoms made of core-shell plasmonic nanoparticles," Langmuir **29**(5), 1551–1561 (2013).
8. A. Merlin, J.-B. Salmon, and J. Leng, "Microfluidic-assisted growth of colloidal crystals," Soft Matter **8**(13), 3526–3537 (2012).
9. T. Nakamura, H. Fuji, N. Juni, and N. Tsutsumi, "Enhanced coupling of light from organic electroluminescent device using diffusive particle dispersed high refractive index resin substrate," Opt. Rev. **13**(2), 104–110 (2006).
10. D. W. Mosley, K. Auld, D. Conner, J. Gregory, X. Q. Liu, A. Pedicini, D. Thorsen, M. Wills, G. Khanarian, and E. S. Simon, "High-performance encapsulants for ultra high-brightness LEDs," Proc. SPIE **6910**, 691017, 691017-8 (2008).
11. K. C. Krogman, T. Druffel, and M. K. Sunkara, "Anti-reflective optical coatings incorporating nanoparticles," Nanotechnology **16**(7), S338–S343 (2005).
12. J. L. Regolini, D. Benoit, and P. Morin, "Passivation issues in active pixel CMOS image sensors," Microelectron. Reliab. **47**(4-5), 739–742 (2007).
13. P. Massé, S. Mornet, E. Duguet, M. Tréguer-Delapierre, S. Ravaine, A. Iazzolino, J.-B. Salmon, and J. Leng, "Synthesis of size-monodisperse spherical Ag@SiO2 nanoparticles and 3-D assembly assisted by microfluidics," Langmuir **29**(6), 1790–1795 (2013).

#192887 - $15.00 USD Received 25 Jun 2013; revised 9 Sep 2013; accepted 23 Sep 2013; published 1 Oct 2013

14. C. Fernández-López, C. Mateo-Mateo, R. A. Alvarez-Puebla, J. Pérez-Juste, I. Pastoriza-Santos, and L. M. Liz-Marzán, "Highly controlled silica coating of PEG-capped metal nanoparticles and preparation of SERS-encoded particles," Langmuir **25**(24), 13894–13899 (2009).
15. H. Fujiwara, Spectroscopic Ellipsometry: Principles and Applications, John Wiley and Sons Inc (2007).
16. G. E. Jellison and F. A. Modine, "Parametrization of the optical functions of amorphous materials in the interband region," Appl. Phys. Lett. **69**(3), 371–373 (1996).
17. J. Tauc, R. Grigorov, and A. Vancu, "Optical properties and electronic structures of amorphous germanium," Phys. Status Solidi **15**(2), 627–637 (1966).

1. Introduction

The demand for specific and peculiar optical properties that do not necessarily exist in natural materials arises in various domains that involve advanced optoelectronics. Optical metamaterials (OMMs) provide an excellent opportunity to tackle this demand by addressing their design at two different scales. On the one hand, the microscopic response of metamaterials can be tailored by carefully selecting and arranging individual nanostructures at the sub-wavelength scale. On the other hand, by organizing the individual resonators into a specific patterned layer and by subsequently stacking these layers together, the metamaterials reach a macroscopic regime. In this regime, the assembled medium can unambiguously be considered as homogeneous and thus exhibits an effective index of refraction. It is worth noting that in order for the assembled structures to qualify as homogeneous optical materials, two important conditions have to be met. First, the typical size a of the elementary cell needs to be smaller than the operating wavelength λ to justify homogenization. Second, the structure must have a thickness h that is large enough for it to be considered as bulk. *Soukoulis et al*. [1] provided an interesting discussion on how large a sample should be to reach the 3D-regime. It was argued that the bulk limit for a metamaterial is reached when the retrieved effective parameters extracted from optical measurements no longer depend on h. In 2008, OMMs made a firm transition from mere metasurfaces to actual bulk materials [2] and the ratios λ/a, which characterizes homogeneity, and h/a, which characterizes bulkiness, may be regarded as two important figures of merit (FOM) that should be as large as possible to assess OMMs.

The top-down fabrication platforms are well suited to precisely control the subwalength dimensions of the individual building blocks of the OMMs. However, they seem to be ill-adapted to reach large h/a values. Up to now, most achievements rarely exceed $h/a \sim 10$ and $\lambda/a \sim 5$ [2–5]. Moreover, most of these metamaterials operate in the near infrared with rare exceptions, such as *Xu et al*. [5] who built a device earlier this year, that demonstrates an all-angle negative refraction of ultraviolet light with modest $h/a \sim 3$ and $\lambda/a \sim 2.3$. Bottom-up fabrication, which combines chemical synthesis and self-assembly, offers an interesting alternative to build bulk OMMs [6,7]. In contrast to the top-down, bottom up procedures allow one to achieve a considerable improvement in the bulkiness ratio without compromising the elementary cell structure.

Here we present bulk OMMs assembled by a recently developed microfluidic evaporation scheme [8] which improves the bulkiness FOM by at least one order of magnitude reaching $h/a > 600$. Moreover, the homogeneity FOM achieved with our best assembled material is $\lambda/a \sim 40$. These OMMs are composed of gold or silver nanoparticles of cubic or spherical shapes as well as metal-dielectric core-shells. The localized surface plasmon resonance of these nanoobjects produces a strongly dispersive effective medium response when they are assembled. The geometry, size, metal-type and volume fraction of metal in the assembled medium all matter and constitute degrees of freedom to engineer the desired index of refraction. The fabricated OMMs demonstrate high refractive index values with low absorption at the red-end of the visible spectrum and in the near-infrared. This property could be of interest for several applications such as high light-extraction substrates and encapsulants for ultra-bright OLEDs [9,10], sensors, telecom devices, antireflective coatings for advanced optical applications [11] or even micro-lens components for CCD, CMOS and CIS devices [12]. Furthermore, an important feature of our fabrication technique is that the resulting OMMs are conveniently contained in microfluidic channels and are ready to be used for

#192887 - $15.00 USD Received 25 Jun 2013; revised 9 Sep 2013; accepted 23 Sep 2013; published 1 Oct 2013

fabrication of bulk optical devices. In addition, the high quality of the surfaces of the fabricated OMMs allows an easy optical characterization using spectroscopic ellipsometry.

2. Synthesis and assembly

We synthesize four types of nanoparticles: silver nanocubes (Ag-CU), Ag@SiO_2 cores-shells (Ag-CS), gold nanospheres (Au-SP) and Au@SiO_2 core-shells (Au-CS). For details on the synthesis of the nanoparticles, readers should refer to Ref [13]. for the Ag-CU particles and to Ref [14]. for the gold particles. The Ag-CS nanoparticles were purchased from NanoComposix and the size data are provided by the manufacturer. Figure 1(a-d) provides pictures of all the nanoparticles in solution. The Ag-CUs are 30 ± 1 nm in size. The Ag-CSs have a 50 nm ± 5 nm cored diameter with a silica shell thickness of 25 ± 5 nm. The Au-SPs are 13.5 ± 1 nm in diameter and are capped with a 5 kDa thiol-PEG ligand. The Au-CS have a 15.2 ± 2 nm core-diameter and a silica shell thickness of 8.5 ± 1 nm.

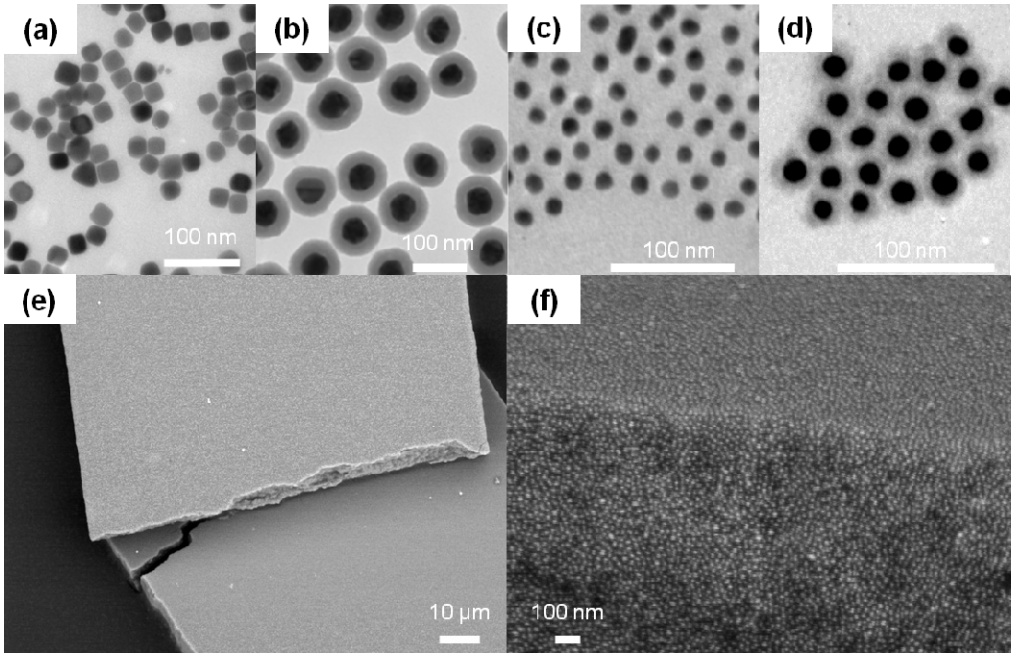

Fig. 1. Images of the nanoparticles and bulk optical metamaterials. TEM images of the individual metallic nanoresonators: (a) Ag cubes, (b) Ag core-shells (©Nanocomposix), (c) Au spheres and (d) Au core-shells. Typical SEM images of the metamaterials assembled via microfluidic evaporation: (e) slab of Ag core-shells and (f) close-up side-view of the edge of a slab of the assembled Au spheres.

The assembly technique we use is based on microfluidic evaporation and is described in length elsewhere [13]. In brief, using standard soft lithography, we fabricate a 10 µm × 100 µm × 10 mm rectangular microchannel. The channel is put in contact with a semi-permeable membrane and is connected to a reservoir (10-50 µL) containing the dilute dispersion. The solvent we use – in this work water – can evaporate across the membrane while the nanoparticles do not and therefore become trapped. As a result, the nanoparticles accumulate in the microchannel. Upon sufficient accumulation time, a dense state of nanoparticles nucleates and invades the channel as it is continuously fed with from the reservoir. Interestingly, the solid adopts the *exact* shape of the microchannel in which it grows and thus exhibits flat interfaces and at least one long dimension. Typical pictures of the assembled OMMs are shown on Fig. 1(e,d). They have channel dimensions: a width of 100 µm, a depth h = 10 µm and are several millimeters long. As can be seen, the fabricated OMMs show very little surface roughness. A structural analysis using micro-focused X-ray scattering (not

#192887 - $15.00 USD Received 25 Jun 2013; revised 9 Sep 2013; accepted 23 Sep 2013; published 1 Oct 2013

shown) demonstrates a limited local order. Therefore, we assume that the assembly is randomly close-packed so that the inter-particle distance is very small compared to the wavelength. In addition, if we consider an operation wavelength of λ = 600 nm which coincides (see section 4) with the localized plasmon resonances of the assembled Ag-CUs and Au-SPs, we find that the homogeneity FOM for our OMMs is equal to λ/a ~20 in the case of Ag-CUs. The same ratio is equal to 10 for the Ag-CS sample and reaches an impressive value of 40 for the case of the Au-SP and Au-CS nanoparticles. Furthermore these OMMs have a high degree of bulkiness with the ratio h/a ~300 for the Ag-CUs, h/a ~200 for the Ag-CSs and h/a ~600 for the gold samples. The large dimensions of the OMMs make them easy to characterize with spectroscopic ellipsometry.

3. Ellipsometric characterization

The optical measurements for the silver nanonoparticle OMMs are made using a Horiba Scientific ellipsometer at two incident angles θ = 60° and 70° in the 350-860 nm wavelength range. The incoming spot size is 80 μm. For the gold nanoparticle OMMs, the measurements are made with a J.A. Woollam ellipsometer in the 240-1000 nm wavelength range with a spot size of 30 μm. Each time, we acquire the spectrum of the complex ellipsometric quantity $\rho = r_p/r_s = \tan(\psi)\exp(-i\Delta)$ where r_p and r_s are the reflection coefficients for p- and s-polarized light, respectively, and (ψ, Δ) are the ellipsometric angles.

For light reflected by a bulk semi-infinite homogeneous and isotropic material, r_p and r_s are simply given by the Fresnel coefficients and the optical index $N = n + ik$ is expressed as a function of ρ. In this case the retrieval of N is immediate and the solution is unique. Therefore, when the incident medium is air, N is unambiguously given by:

$$N = \sin\theta\left\{1+\left(\frac{1-\rho}{1+\rho}\right)^2 \tan^2\theta\right\}^{1/2}, \qquad (1)$$

where θ is the angle of incidence [15].

As was discussed in section 2, each sample is made of nanoparticles assembled in random close-packing order, so that the dimensions of the nanoresonators and their spacing are very small compared to the wavelength and the material is highly homogeneous. For each sample, we proceed in the same manner. The microchannels are 10 μm deep and the underlying medium is a semi-infinite PDMS substrate for which the optical properties are measured independently. First, we perform a numerical inversion using a multi-layer model containing the 10 μm OMM on top of the PDMS substrate and make sure that the retrieved N is identical to that found using Eq. (1). The fact that both indices of refraction coincide indicates that the OMM is indeed an optically semi-infinite medium. As a result, measuring ρ and using Eq. (1) can be regarded as a direct measurement of $n(\lambda)$ and $k(\lambda)$. The measured spectra $n(\lambda)$ and $k(\lambda)$ are represented by blue and red dots respectively in Fig. 2. Second, to check that our measured N are physical, we fit the ellipsometric parameters (ψ, Δ) using two Lorentz-oscillators (LO) to describe the dielectric constant ε of our MM. The dispersion relation given by the LO model classically describes the collective electron oscillations of localized surface plasmon resonances that occur in metallic nanoparticles embedded in a dielectric host medium. Since the vicinity of each resonator is slightly different from one particle to another because of the randomness of the fabrication technique, so are the width and position of the individual responses. For this reason, a single LO may be insufficient to accurately fit the experimental data. For each medium the model used for the ω-frequency dependence of ε is

$$\varepsilon(\omega) = \varepsilon_\infty + \sum_{j=1}^{2} \frac{f_j \omega_{0j}^2}{\omega_{0j}^2 - \omega^2 + i\gamma_j\omega}, \qquad (2)$$

where f_j, ω_{0j} and γ_j are the oscillator strength, resonance frequency and damping constant. ε_∞ is a constant. As the UV frequencies are approached, this classical model decreases in

#192887 - $15.00 USD Received 25 Jun 2013; revised 9 Sep 2013; accepted 23 Sep 2013; published 1 Oct 2013

accuracy because of the interband transitions in the metal. For this reason, we append a Tauc-Lorentz oscillator (TLO) to Eq. (2), which was initially proposed by Jellison and Modine [16] and is accurate in describing the interband absorption. The Tauc-Lorentz model consists in multiplying the imaginary part of the dielectric function obtained from the Lorentz equation by the Tauc joint density of states [17]. Even though it was originally proposed to describe amorphous semiconductors, we observe empirically that it provides a reasonable fit to optical properties of metallic nanocomposites at the UV end of the visible spectrum. The data are fitted by using the χ^2-test. The fitted curves are represented by continuous lines in Fig. 2.

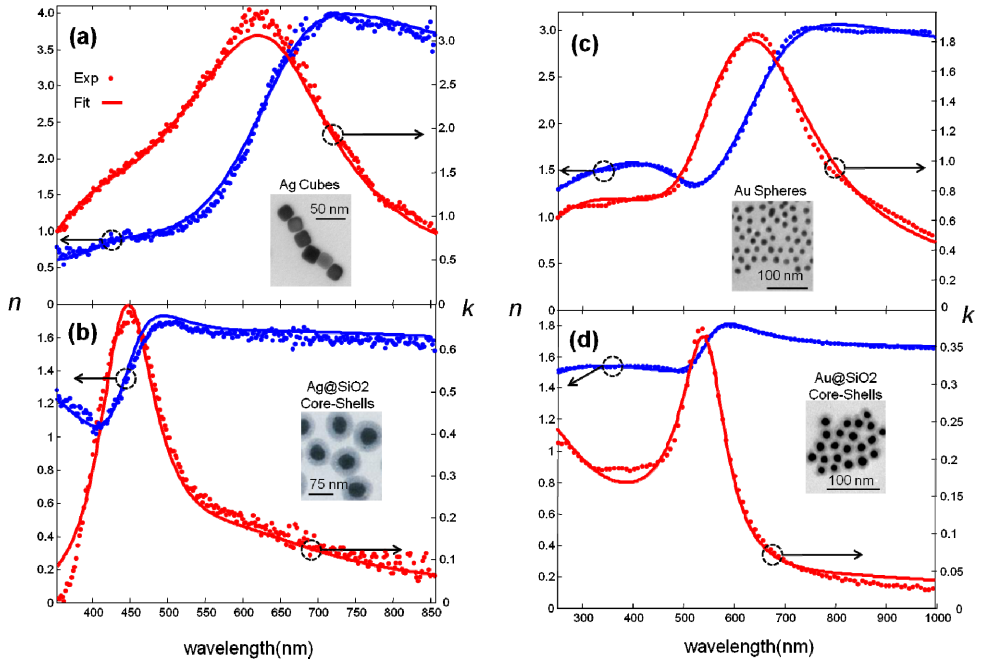

Fig. 2. Optical Properties of the bulk optical metamaterials. Each graph shows the spectral evolution of the measured real (blue) and imaginary (red) part of the optical index $N = n + ik$ for assembled (a) Ag cubes, (b) Ag core-shells, (c) Au spheres and (d) Au core-shells. Dots represent the values obtained by measuring $\rho(\lambda)$. The continuous lines represent the fits using the Lorentz-oscillator models for the dielectric constant of the metamaterial.

4. Results

Figure 2 shows the typical optical properties of the fabricated OMMs and compares the optical index N retrieved from Eq. (1) (dots) with the fitted models (continuous line) for the four types of nanoparticles. We can see that the agreement between the model and the retrieval data is excellent for all types of nanoparticles. Table 1 summarizes the converged fitting parameters for each OMM. The TLO parameters are described using the notations given in Ref [16]. From Table 1 we conclude that the main plasmon resonance of the assembled silver cubes and core-shells is observed at $\lambda_{Ag\text{-}CU} = 616$ nm and $\lambda_{Ag\text{-}CS} = 450$ nm with full-widths at half-maximum $\Delta\lambda_{Ag\text{-}CU} \sim 290$ nm and $\Delta\lambda_{Ag\text{-}CS} \sim 160$ nm respectively (see Fig. 2). It is interesting to note that the Ag-CU sample sees its resonance red-shifted and broadened by larger amounts compared to the resonance of unassembled Ag-CU nanoparticles when they are in solution ($\lambda'_{Ag\text{-}CU} = 412$ nm, $\Delta\lambda'_{Ag\text{-}CU} \sim \Delta\lambda_{Ag\text{-}CU}/2.5 = 116$ nm). Such significant changes of the resonance properties come from the strong inter-particle coupling which is large due to the random close-packing of the nanocubes in the OMM. At the same time, the Ag-CS sample has its resonance at exactly the same position as that of individual nanoparticles and the broadening of the resonance induced by inter-particle interactions is relatively small ($\lambda'_{Ag\text{-}CU} = \lambda_{Ag\text{-}CU}$, $\Delta\lambda_{Ag\text{-}CU} \sim \Delta\lambda_{Ag\text{-}CS}/1.5 = 107$ nm). This can be

#192887 - $15.00 USD Received 25 Jun 2013; revised 9 Sep 2013; accepted 23 Sep 2013; published 1 Oct 2013

explained by the fact that, contrary to the Ag-CU samples, the inter-particle coupling in core-shell OMMs is weak due to the presence of a sizable silica shell which has a thickness almost equal to the silver core radius and keeps the silver cores apart. The gold samples exhibit similar behavior. These observations suggest a relatively simple way in which, by controlling particle sizes and inter-particle separation, it is possible to engineer the dispersion of an OMM. The core-shell samples have a refractive index which rises rapidly from $n_{Ag\text{-}CS} = 1.2$ to $n_{Ag\text{-}CS} = 1.6$ in the 400-500 nm band for Ag-CSs and from $n_{Au\text{-}CS} = 1.5$ to $n_{Au\text{-}CS} = 1.66$ in the 500-600 nm band for the Au-CSs. For higher wavelengths, the value of $n \sim 1.6$ is maintained across the rest of the visible spectrum and well toward infrared wavelengths, while the absorption slowly decreases reaching impressively low values (e.g. $k_{\text{Au-CS}} \sim 0.02$). The Ag-CU and Au-SP samples present a similar evolution except that the refractive index n rises across the visible spectrum from low values (0.5 and 1.3 respectively) to very large values (3.7 and 3 respectively) at 700 nm with decreasing absorption above 650 nm well into the IR.

Table 1. OMM Parameters fitted by the spectroscopic model. **(Frequencies are given in eV)**

Param.	**Ag Cubes**	**Ag Core-Shells**	**Au Spheres**	**Au Core-Shells**
ε_∞	2.3	1.44	2.18	1.90
N° of LOs	2	2	1	1
(f_j, ω_{0j}, γ_j)	(5.5, 1.88, 0.56) (0.53, 2.89, 1.2)	(0.36, 2.73, 0.49) (0.17, 2.0, 1.12)	(0.23, 2.3, 0.51)	(0.64, 6.19, 5.78)
TLO	No	Yes	Yes	Yes
(E_g, A, E, C)	–	(3.58, 300, 2.41, 0.9)	(1.67, 11.24, 4, 6.23)	(1.56, 4.24, 2.23, 0.43)

5. Conclusion

The combination of nanochemical engineering and microfluidic self-assembly enables us to obtain homogeneous optical metamaterials with a high degree of bulkiness exceeding the state-of-the-art realizations by at least one order of magnitude. Our fabrication technique enables a rapid and easy characterization using spectroscopic ellipsometry and allows one to make optical devices, such as lenses, filters, modulators using suitable thin plastic molds and filling them with nanoparticles. We obtain OMMs that reach high refractive index and low absorption in the deep red and the near-IR. We foresee that the combination of these two techniques will considerably reduce the complexity in the experimental investigations of bulk optical metamaterials, notably in the quest for optical magnetism. This leaves nanochemical synthesis and nanoparticle design at the heart of the study of three-dimensional OMMs.

Acknowledgements

This work was supported by the European FP7 project METACHEM under grant #228762. A. Baron acknowledges the AMADEUS Labex for financial support.

#192887 - $15.00 USD Received 25 Jun 2013; revised 9 Sep 2013; accepted 23 Sep 2013; published 1 Oct 2013